Analysis of Large Civil Tilt Rotor Wind Tunnel Blockage and Validation Using RotCFD

S. Esma Sahin
Research Associate
Science and Technology Corporation
Moffett Field, CA, USA

Carl R. Russell
Aerospace Engineer
NASA Ames Research Center
Moffett Field, CA, USA

Eduardo Solis
Design Engineer
Monterey Technologies, Inc.
Moffett Field, CA, USA

R. Ganesh Rajagopalan
Professor
Iowa State University
Ames, IA, USA

ABSTRACT

Ground based experiments are often used to understand and measure rotor and airframe aerodynamic performance; however, these experiments have certain limitations. The effects of these limitations are evaluated here using computational fluid dynamic (CFD) modeling techniques. Through this study, data from the 7- by 10-Foot Wind Tunnel experiments of the Large Civil Tilt Rotor (LCTR) at NASA Ames Research Center is validated using CFD. The Reynolds Averages Navier-Stokes solver, RotCFD, is used for the computations. In particular, the effect of the blockage generated by the test hardware on the walls is investigated. To study this problem, simplified geometries such as a flat plate, cube and cylinder are also investigated for blockage effects. This is done to explore if these different geometries can represent the LCTR as a simplified case to reduce computational time and get a quick first understanding of tunnel blockage effects. The focus of this research is to understand the limitations and accuracy of the recent small-scale Large Civil Tilt Rotor wind tunnel test campaigns.

INTRODUCTION

The Large Civil Tilt Rotor (LCTR) is a civil transport aircraft that can vertically takeoff and land. It was developed as part of the NASA Heavy Lift Systems Investigation and it is designed to carry 90 passengers for 1000 nm at 300 knots (Ref. 1).

The concept of the LCTR is to free up the runways by moving short- and medium-range air traffic to helipads, which will allow the main runways to be used by a larger number of long range aircraft. This will increase the capacity of the airspace because more aircraft can take off within a certain time. The Vertical TakeOff and Landing (VTOL) aircraft will use existing helipads nearby the airport, therefore new constructions will not be needed (Ref. 2).

The objective of the LCTR2 design studies is to identify research requirements for future tiltrotors (Ref. 2). Areas of investigation to date are wind tunnel tests in the US Army's 7- by 10-Foot Wind Tunnel at NASA Ames Research Center, water tunnel tests in the Ames Fluid Mechanics Lab, and CFD calculations using RotCFD, a software package developed through a joint collaboration between NASA and Sukra Helitek Inc. The main aim of this project is to validate the 7- by 10-Foot Wind Tunnel experimental test results of the LCTR at NASA Ames Research Center with RotCFD, to investigate the limitations of ground based testing.

This paper gives some background information about previous experimental work. After this the LCTR2 design study is given, followed by the RotCFD analyses. The final part includes the results.

PREVIOUS EXPERIMENTAL WORK

In 2005, the NASA Heavy Lift Rotorcraft Systems Investigation (Ref. 3) identified the Large Civil Tiltrotor (LCTR) as the configuration with the best potential to meet the technology goals of the NASA Vehicle Systems Program for large civil transport (Ref. 2).

NASA's Large Civil Tilt Rotor (LCTR) and the Army's High Efficiency Tilt Rotor (HETR) were tested by NASA and the U.S. Army during the wind tunnel test program in April 2012 and October 2013 (Ref. 4). Both of the tiltrotors were modeled at 6% scale and had no rotors on throughout the tests in the 7- by 10-Foot Wind Tunnel at NASA Ames Research Center. The main similarity between the two models is that the HETR wing and nacelle geometries were incorporated into the LCTR scale model. An overview of the LCTR geometry is given in Fig. 1.

The LCTR model was tested in airplane mode at high speed with a Reynolds number range of 0.8 to 1.4 million and in helicopter mode at low speed with a Reynolds number range of 0.3 to 0.6 million, where the inner wing chord was used as reference length. This corresponds to Mach number ranges of 0.17 to 0.31 and 0.06 to 0.13, respectively. During the tests in airplane mode, the angle of attack ranged from -10 to

Presented at the AHS International Technical Meeting on Aeromechanics Design for Vertical Lift, San Francisco, California, January 20–22, 2016.

+12 deg., and the sideslip angle from 0 to +10 deg. In helicopter mode, the model was tested at yaw angles from -180 to +180 deg. The nacelles were at a zero-degree angle for the high-speed measurements (airplane mode) and under a varying angle from 60 degrees to 95 degrees for the low-speed testing (helicopter mode).

To minimize the effect of the presence of the struts on the measured aerodynamic forces and moments, two sets of fairings were installed covering the struts. Aerodynamic shaped fairings were used for high-speed measurements (airplane mode), and circular fairings were used for low-speed measurements where large yaw angles were tested (helicopter mode).

The full LCTR airframe model testing included three wing tip configurations; a wing cap (nacelle and extension removed), a nacelle only (wing extension removed) and a wing extension with nacelle. The wing only model was only tested in airplane mode for the range of velocities at Mach 0.06 to 0.30, again at different wing tip configurations (Ref. 4).

The objective of the wind tunnel test was to validate the CFD tool and the performance predictions made during conceptual design, and to develop flight dynamics simulation models. The results also gave insight into the aerodynamic performance of the LCTR2 and its wing, with a focus on the wing extensions and the nacelles. The current study focuses on how accurate and robust these wind tunnel tests are by comparing selected wind tunnel data with the CFD computations.

THE LCTR2 DESIGN STUDY

In this section, the different areas that are investigated are given.

Validation of Experimental Data Through Correlation

The wind tunnel test was performed in the U.S. Army 7- by 10- Foot closed return wind tunnel at NASA Ames Research Center. The 7- by 10-ft. test section is rectangular in shape with a constant height of 7ft. The width increases linearly from an initial value of 10.01 ft. to a final value of 10.1335 ft. over the test section length of 15 ft. to allow for boundary layer growth (Ref. 6). While modeling the tunnel walls in RotCFD, this increase in width is not taken into account. A series of pressure orifices are located in the walls of the contraction cone a short distance upstream of the test section. The tunnel has 3 static pressure rings, with each ring consisting of 4 static-pressure orifices, two on each side wall. The pressure rings differ in upstream location. Generally, the first pressure ring is used, but this can be replaced by the second or third, depending on the blockage of the model.

The flow past an object is constrained by blockages because it is bounded by solid walls. During wind tunnel testing, these walls disturb the airflow around the model. The effect is an increase in the freestream velocity. This can be correlated to the volume distribution of the model itself (solid blockage), and to the displacement effect of the wake (wake blockage) (Ref. 7). The blockage effects in the wind tunnel also arise from the influence of model supports like fairings and struts within the airstream. The LCTR model has two types of fairings and struts that are changed according to the configuration. The current blockage study shows the influence of the fairings and struts on the flow field. Furthermore, the LCTR in helicopter mode causes a large blockage in the wind tunnel. Attention, therefore, is paid to the side wall pressure distribution. The different wind tunnel wall effects can influence the wind tunnel data. By using CFD it can be investigated if corrections are needed for the wind tunnel data.

The validation of the wind tunnel data is being performed with Rotorcraft Computational Fluid Dynamics (RotCFD) (Ref. 8). The key components of RotCFD are a geometry module, a grid generation module, a Navier-Stokes flow-solver module, a blade element rotor module, and a flow visualization and analysis module. The governing equations of the incompressible, unsteady flow are modified in order to incorporate turbulence by time-averaging the Navier-Stokes equations. This leads to the well-known Reynolds Averaged Navier-Stokes Equations (Ref. 9). To account for the inherent turbulent nature of rotorcraft flows, the Realizable and Standard ‘k-epsilon’ model have been integrated to the RotUNS flow solver. This model has a special treatment for wall boundaries. The two-equation model chosen here is the Realizable ‘k-epsilon’ model. The k-epsilon model is applicable to free-shear layer, wall-bounded and internal flows with relatively small pressure gradients (Ref. 10).

In this study, primary attention is paid to the side wall pressure distributions when there is a large blockage in the tunnel (particularly at yaw angles approaching 20 deg.). This is done by comparing CFD predictions of the LCTR2 model with and without wind tunnel walls to the wind tunnel test data. This determines the extent of wind tunnel wall effects on the measured data that might cause the measured tunnel results to not accurately reflect free flight aerodynamic performance of the model. In order to do this, the aerodynamic moments and forces can be compared together with the pressure distribution along the tunnel walls. Also, a comparison is made between the pressures measured at the pressure ring locations in the settling chamber upstream of the test section for blockage effects.

Rotor Aerodynamic Interaction with Airframe

When the full airframe model in CFD has been validated, rotors will be added to the model to perform an analysis. RotCFD will be used to model the two rotors. In the unsteady rotor modeling technique, the rotor is modeled as discrete rotor blades. By performing an analysis with a rotor configuration, the aerodynamic interactions between the

rotor wake and the airframe can be predicted to enable performance and loads predictions with rotor interactions (Ref. 11).

Simplified Geometries

Different geometries that have the same blockage as the LCTR are simulated in RotCFD to study if a simplified body has the same blockage effect. The different geometries that are evaluated are a square flat plate, rectangular flat plate, cube, rectangle, and cylinder. To simulate these geometries, the blockage of the LCTR at different configurations and angles was calculated. The first two cases represent the LCTR at a yaw angle that gives the minimum and maximum blockage.

The LCTR was tested in airplane and helicopter mode. Calculating the blockage at different yaw angles results in a minimum blockage at 0 degrees in airplane mode and a maximum blockage at 70 degrees yaw angle in helicopter mode. In Table 1 the blockage ratios for both cases can be found.

Dye Flow Water Channel Tests

The NASA Ames Fluid Mechanics Lab Water Channel (Ref. 12) was used to visualize the flow around the LCTR in airplane and helicopter mode, with and without rotors, and the simplified geometries. The LCTR in airplane mode and some of the simplified geometries are given in Fig. 3A-D.

The water channel allows one to have a quick view of the streamlines and wake of the model while keeping the costs low. During the test, a yellow-green fluorescent dye solution is injected upstream of the model. To visualize the separated flow region, red dye is injected downstream of the model. Four UV lamps illuminate these dyes. In Figure 2A-C, the LCTR model and the simplified geometries are shown. All the tests have been done at various pitch and yaw angles.

ROTCFD ANALYSES

In this section the test cases that are used for the validation study are given. This is followed by the grid and convergence study.

Test Cases

The wind tunnel data has been studied carefully to choose the LCTR test configurations that will be validated with RotCFD. As mentioned before, it was decided to choose the configurations with the smallest and largest blockage, respectively; the airplane mode in 0 degrees yaw and helicopter mode in 70 degrees yaw. The nacelle angle with respect to the camber line is chosen to be 85 degrees in helicopter mode, since this configuration has the most data points. For completeness, the helicopter mode is also simulated in 0 and 90 degrees yaw. The data sets for these configurations are chosen such that the Mach number is not too high in order to solve the problem in RotCFD, have many data points, and a wide angle of attack or yaw angle. The latter two are done to be able to use the same test run in case different angles need to be solved in the future. Also, the forces and moments of the LCTR with and without wing extension for the chosen configurations were compared. The LCTR without wing extension is only simulated when the difference is significant. In Table 2, the values of the velocity, Reynolds number and Mach number, for the airplane and helicopter mode are given. In Table 3 and 4 the test cases and the comment for each case can be found. The numbers in Table 3 represent the test cases that are done, and the letters are the cases that are not done.

Grid Study

For the time settings within RotCFD, the time length, time steps, iterations, and relaxation can be set. The (delta) time step size can be calculated by dividing the smallest cell size by the velocity at that point in the wind tunnel. Dividing the time that a particle needs to flow from the inlet to the outlet by this time step size, gives the amount of time steps needed.

Grid generation is the trickiest part of CFD. Therefore, the recommendation is to start with a non-body-fitted grid to get a quick impression of the results and the settings. After this step, the grid is refined by starting with a coarse body-fitted grid. Finer grids give more accurate results, but with accuracy comes longer solving time.

The airplane mode configuration with wind tunnel walls is used to find the proper grid settings. The time step size was set at (1/32)ft / 284.21ft/s = 0.0001s and the number of time steps at 0.1s / 0.0001s = 1000. The simulation was started with 10 iterations and a relaxation of 0.1, but changed accordingly to 20 iterations and relaxation of 0.01 as a result of divergence of the solutions. Also, the refinement box around the model was increased from 1 to 3. Once the non-body-fitted setting worked, the same settings were applied to the body-fitted grid and improved. Again, the iterations, relaxation and refinement box were changed one at the time until the right setting were found. The two time step sizes that are investigated hereby are 0.0001 and 0.00003. The former is the calculated time step size and the latter is the calculated time step size by using the time and the time step of the non-body-fitted case as a constraint. A recommendation is to try time step sizes between 0.0001 and 0.0003 and relaxation between 0.1 and 0.01, which is not done due to time constraints.

The preliminary results of these test cases were plotted to show grid independency. It is noted that convergence is reached faster when the iteration is increased. Therefore, the best test case was chosen and improved by varying the iteration and the time step size.

Convergence Study

After running the second test set, the settings that showed the best results were used for all the configurations: 2.5s time length, 5000 time steps, 0.0005s time step size, 50

iterations, and 0.01 relaxation. However, even after reaching good and fast results, the solution diverged at the time step where it almost reaches convergence. The divergence is probably caused by stability issues with the turbulence model when it encounters poor quality body-fitted grid cells. The diverging turbulence values are coupled back into the flow equations resulting in eventual flow field divergence. It is difficult to improve the quality of the grid cells because grid refinement results in a significant increase in simulation time. To solve the problem, the turbulence relaxation factors were varied for one test case, the LCTR in airplane mode in freestream conditions. The simulation was restarted from the time step that shows no error yet. The error will typically manifest in the turbulent dissipation (epsilon) residual starting to 'run-away', followed by the turbulent kinetic energy (TKE) residual. Restarting the simulation before the solution diverges saves time but is tricky, as the instability may already exist in the restart file. Attention is needed to ensure that the restart time is as long as possible before any indication that the case is going bad, given one's run-time constraints. The initial turbulence relaxation factors, k relaxation factor and epsilon relaxation factor, are set to 0.9 and 0.7, respectively. Three factors that were chosen to be tested are 0.1, 0.3 and 0.5. The best results are obtained with the 0.3 factor, so 0.3 is applied to all the configurations. The difference between the three turbulence relaxation factors is shown in Fig. 4 by marks at the divergence point of each relaxation factor. In this figure the total force for the four different turbulence relaxation factors is plot against the time step.

The initial turbulence relaxation factor, 0.9-0.7, gives the worst results with a divergence at 840 time steps. The residual plot in Fig. 5 shows that at 500 time steps the error has not started yet, so this point is a save choice to restart the simulation with the other factors. The second divergence occurred at 850 time steps with a factor of 0.5. Using a factor of 0.1 gives a divergence at 930. The best results are obtained with a factor of 0.3 since this delays the divergence to 1510 time steps. The residual plot of this can be seen in Fig. 6.

Using this turbulence relaxation factor does delay the divergence point but does not solve it. To further improve the results, or reach convergence, the time step size is varied every time an error is observed. The initial time step size is 0.0005 and changed to 0.0001, 0.00005, 0.00001, respectively. This process is different for each configuration; therefore, the time step sizes are changed according to the configuration. A recommendation is to try smaller time step jumps, which is not done due to time constraints. Using the process of changing the time step size, in combination with the adjusted turbulence relaxation factor, solved the divergence problem. In Fig. 7, the change in solution due to the decrement in time step size can be seen. Again, the total force is plotted against the time step and the time step size decrements are marked.

After divergence of the results with the initial time step size, 0.0005, the simulation is restarted at 500 time steps with time step size 0.0001. The time step sizes 0.00005 and 0.00001 are set at 650 and 750 time steps, respectively. The last decrement shows that the solution is converged. This can be also seen in the residual plot, Fig. 8, by observing that the residuals are steady.

As last, the same configuration is also simulated with the smallest time step size that is needed to reach convergence. Figure 9 and 10, the total force and residual plot, respectively, show that the same results are approached as using the time step size decrements process. It is recommended to use the decrement process since this reduces the time significantly.

RESULTS

The wind tunnel blockage and wall effects are given by the force and residual plots of the LCTR in airplane mode. The helicopter mode is not treated in this paper. The developed grid of the LCTR in airplane mode in the 7- by 10-Foot Wind Tunnel at NASA Ames Research Center is given in Fig. 11. The effect of the wind tunnel walls on the forces and moments can be investigated by comparing the LCTR in airplane mode with wind tunnel walls and freestream. By comparing the LCTR with and without wing extension in the wind tunnel, the effect of the wing extension can be studied. The grid of the LCTR without wing extension is illustrated in Fig. 12.

By using the 0.3 turbulence relaxation factor and the time step size decrement method, the final cases, as given in Table 3, can be solved. The calculated forces are the drag (Fx), side force (Fy) and lift (Fz). The calculated moments are the rolling moment (Mx), pitching moment (My), and yawing moment (Mz). In Fig. 13 and 14, the forces and moments together with the residuals are compared for the LCTR in airplane mode in freestream (F) and with wind tunnel walls (W). From these figures, it can be noted that convergence is reached and that in freestream conditions the forces are lower while the moments are higher. However, the residual plot does show that divergence will occur if the simulation will run longer. Restarting with a smaller time step size around the 1000 time steps could solve this. Comparison with the forces and moments of the experimental data shows that the lift force is almost the same as the simulation with wind tunnel walls; all the other forces are closer to the freestream condition. The lift, drag and side force of the experiment are 249.83 lb, 17.91 lb, and 10.76 lb, respectively. The pitching, rolling, and yawing moments are 79.03 lb-ft, -8.64 lb-ft, and 3.24 lb-ft, respectively. The experimental results are marked in Fig. 13. The difference in drag is probably caused by the fairings and struts that are included in the CFD results. The simulations have also been executed without fairings and/or struts, so additional plots could be made by excluding the model supports for a better result. Figures 15 and 16, present the difference of the LCTR with wind tunnel walls, with (W) and without wing

extension (NE). Note that the results for both cases are almost the same, except the lift (Fz) is significant higher with wing extensions. The same as in Fig. 14 holds for the residual plot.

The wind tunnel blockage and wall effects can be also shown by plotting the pressure field along the wind tunnel walls or in the whole flow field. The pressure plots are not treated in this paper. Therefore, the simplified geometry and the empty wind tunnel are not relevant at the moment. This also means that no judgement can be made on the pressure rings.

SUMMARY AND CONCLUSIONS

Wind tunnel effects can occur due to the blockage of the model or wall interference. A validation study is needed in order to investigate if the computed wind tunnel data is correct or that a correction is needed to account for wind tunnel effects.

The CFD tool that is used for the validation study is RotCFD. Previous studies showed that this tool is capable of accurately visualizing the flow field of a rotorcraft and other geometries. RotCFD is a RANS solver where the fluid flow is governed by the incompressible, laminar Navier-Stokes equations. A k-e turbulence model is used, with a turbulence relaxation factor that is adjusted to 0.3 to obtain better results. This factor has been found by trying different numbers from the restart time where an error is observed in the residual plot. To save time, the simulation is restarted from this restart time instead of from the start. The error can be observed from the turbulent dissipation (epsilon) and the turbulent kinetic energy residual plot at the restart time where the graph starts to 'run-away'. To further improve the results the time step size is reduced every time an error is observed with the new time step size. The time step reduction approach is time efficient compared with using the smallest time step for the whole simulation.

Different configurations of the LCTR that are modeled are the airplane mode at one yaw angle and the helicopter mode at various yaw angles. These yaw angles are chosen such that the model causes minimum and maximum blockage in the wind tunnel. The wind tunnel settings for these configurations are obtained from the experimental wind tunnel data. By modeling the LCTR with wind tunnel walls and in freestream, the effect of the blockage generated by the test hardware on the walls is investigated. The wind tunnel blockage and wall effects are observed by comparing the forces and moments on the body and the pressures along the wall and in the test section. Next to this, the LCTR is modeled without wing extension to see the influence of the extension on the wall pressures. Also, a simplified body with the same blockage ratio as the LCTR is modeled to compare the blockage effects. The pressure results are not included in this paper. All results are given for the LCTR in airplane mode; the helicopter mode results are omitted from the paper.

Knowledge in wind tunnel testing for civil tiltrotors is important to improve rotorcraft aerodynamic performance predictions. Civil tiltrotors are gaining interest due to the increasing density of the airspace. Their capability to vertically take off and land makes the aircraft applicable for many purposes. Understanding of the influence of wind tunnel walls on the computed wind tunnel data is needed for future wind tunnel tests.

Author contact: S. Esma Sahin sesahin@live.nl

REFERENCES

[1]Acree, C.W., *"Aerodynamic Limits on Large Civil Tiltrotor Sizing and Efficiency"*, 5th Decennial AHS Aeromechanics Specialists' Conference, San Francisco, CA, January 22-24, 2014.

[2]Young, L., *"Civil Tiltrotor Aircraft Operations"*, 11th AIAA Aviation Technology, Integration, and Operations (ATIO) Conference, Virginia beach, VA, Sept, 2011.

[3]Johnson, W., Yamauchi, G. K., and Watts, M. E., *"NASA Heavy Lift Rotorcraft Systems Studies"*, NASA/TP-2005-213467, December 2005.

[4]Theodore, C.R., Willink, G.C., Russell, C.R., Pete, A.E., Amy, A.R., *"Wind Tunnel Testing of a 6%-scale Large Civil Tilt Rotor Model in Airplane and Helicopter Modes"*, Fifth Decennial AHS Aeromechanics Specialists' Conference, San Francisco, CA, January 22-24, 2014.

[5]Acree, C. W. Jr., *"Integration of Rotor Aerodynamic Optimization with the Conceptual Design of a Large Civil Tiltrotor*", No. 562061, AHS Aeromechanics Conference, San Francisco, CA, January, 2010.

[6]Wadcock, A.J., *"The NASA Ames 7ft. x 10ft. Wind Tunnel – Presesnt Flow Quality and Recommendations for Improvement"*, Final Report Under Modification No.2 to contract NAS2-11945, NASA Ames Research Center, Moffett Field, CA, July, 1987.

[7]Maskell, E.C., *"Theory of the Blockage Effects on Bluff Bodies and Stalled Wings in a Closed Wind Tunnel"*, Reports and Memoranda No. 3400, November, 1963.

[8]Rajagopalan, R. G., Baskaran, V., Hollingsworth, A., Lestari, A., Garrick, D., Solis, E., Hagerty, B., *"RotCFD - A Tool for Aerodynamic Interference of Rotors: Validation and Capabilities"*, Future Vertical Lift Aircraft Design Conference, San Francisco, CA, January 18-20, 2012.

[9]Sukra Helitek, Inc. Ames., *"RotUNS Rotor UNStructured Solver Application RotCFD"*, Iowa, August 7, 2014

[10]Bardina, J.E., Huang, P.G., Coakley, T.J., *"Turbulence Modeling Validation, Testing, and Development"*, NASA Technical Memorandum 110446, 1997.

[11]Rajagopalan, R. G., Baskaran, V., Hollingsworth, A., Lestari, A., Garrick, D., Solis, E., Hagerty, B., *"RotCFD - A Tool for Aerodynamic Interference of Rotors: Validation and Capabilities"*, Future Vertical Lift Aircraft Design Conference, San Francisco, CA, January 18-20, 2012.

[12]Bell, J.H., Heineck, J.T., Zilliac, G., Mehta, R.D., Long, K.R., *"Surface and Flow Field Measurements on the FAITH Hill Model"*, American Institute of Aeronautics and Astronautics.

FIGURES AND TABLES

Table 1. LCTR wind tunnel settings.

	Frontal area [in^2]	Blockage [%]
Wind tunnel	10080	-
Airplane mode - Pitch: 0 deg., Yaw: 0 deg.		
Model only	220.444	2.187
Model with aerodynamic struts and fairings	662.712	6.575
Helicopter mode - Pitch: 0 deg., Yaw: 70 deg.		
Model only	665.770	6.605
Model with circular struts and fairings	1358.497	13.477

Table 2. LCTR wind tunnel settings.

Configuration	Velocity [m/s]	Reynolds Number [-]	Mach Number [-]
Airplane Mode	284	1.20×10^6	0,26
Helicopter Mode	140	0.60×10^6	0,12

Table 3. LCTR test cases.

Configuration	Case	LCTR with wing extensions	LCTR without wing extensions	No model	Flat plate	With walls	Without walls
Airplane mode – Pitch: 0 deg., Yaw: 0 deg.							
	1	x				x	
	2	x					x
	3		x			x	
	4			x		x	
	5				x	x	
	6				x		x

Helicopter mode – Pitch: 0 deg., Yaw: 70 deg.							
7	x					x	
8	x						x
A			x			x	
9				x		x	
10					x	x	
11					x		x
Helicopter mode – Pitch: 0 deg., Yaw: 0 deg.							
12	x					x	
13	x						x
14			x			x	
15				x		x	
B					x	x	
C					x		x
Helicopter mode – Pitch: 0 deg., Yaw: 90 deg.							
16	x					x	
17	x						x
D			x			x	
18				x		x	
E					x	x	
F					x		x

Table 4. Comments on the LCTR test cases.

Case	Comment
1, 3, 7, 12, 14, 16	LCTR with fairings and struts.
2, 8, 13, 17	LCTR without fairings and struts
4, 9, 15, 18	Empty wind tunnel
15, 18	Empty wind tunnel almost same settings as 9 (β=70)
5, 6, 10, 11	Flat plate with same frontal area as LCTR with fairings and struts
6	Flat plate with same frontal area as LCTR with fairings and struts
A, D	Not modeled: Δ due to wing extension is small
B, C, E, F	Not modeled: only modeled for maximum blockage

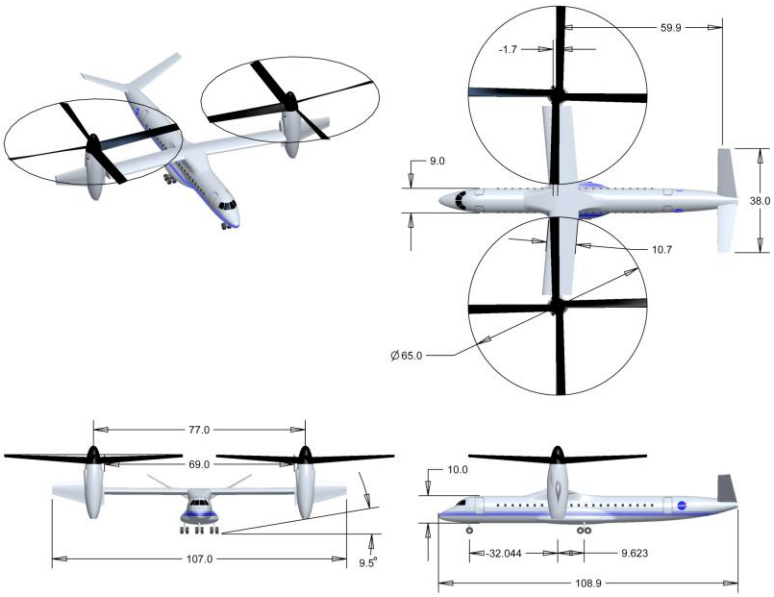

Figure 1. The NASA Large Civil Tiltrotor, LCTR2 baseline version (dimensions in feet) [5].

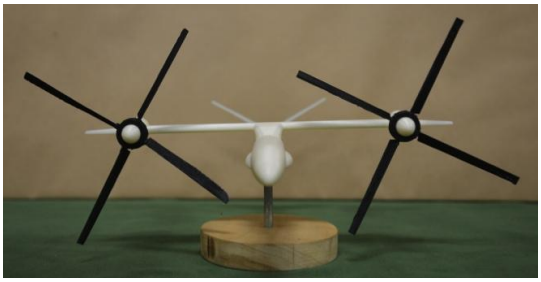

Figure 2A. The LCTR model with rotors in airplane mode.

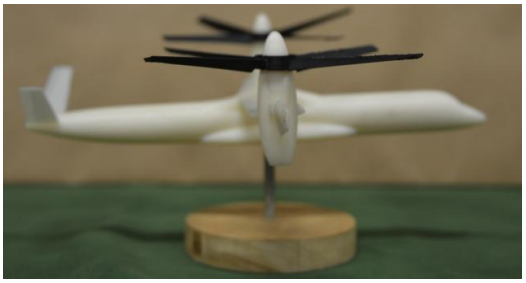

Figure 2B. The LCTR model with rotors in helicopter mode.

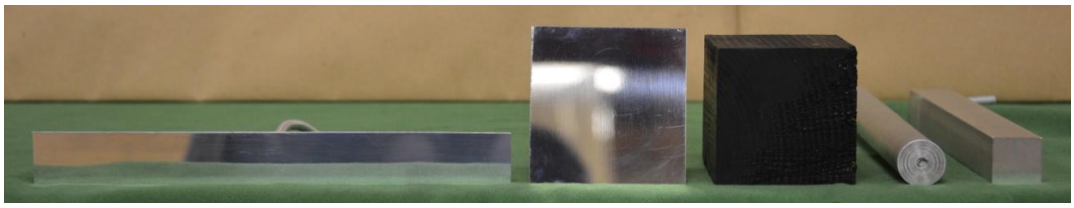

Figure 2C. The simplified geometries: rectangular flat plate, square flat plate, cube, cylinder, and rectangle.

Figure 3A. Water channel results of the LCTR in airplane mode (isometric view).

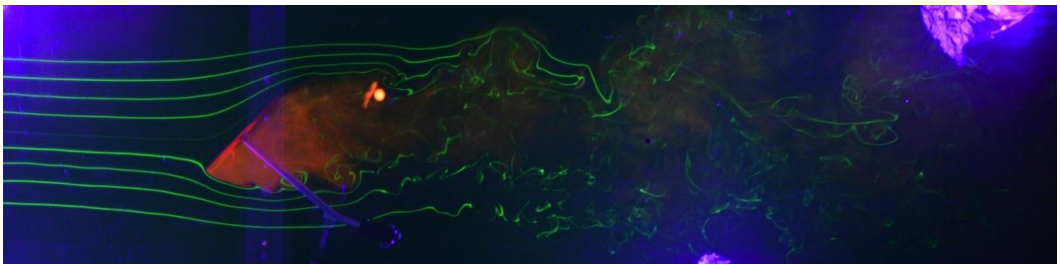

Figure 3B. Water channel results of the flat plate (side view).

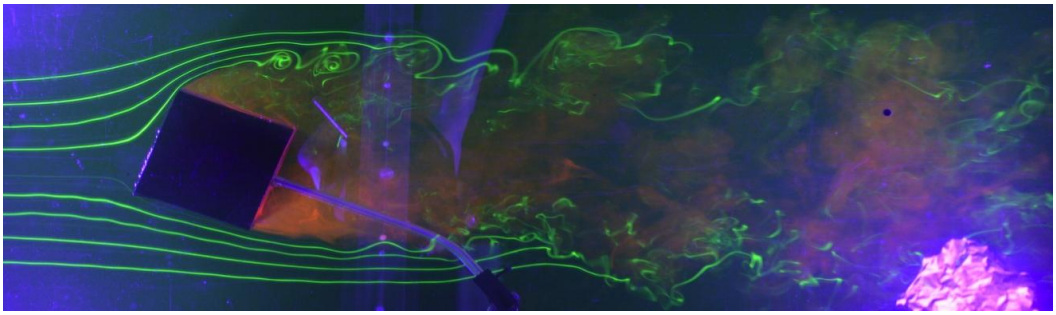

Figure 3C. Water channel results of the cube (bottom view).

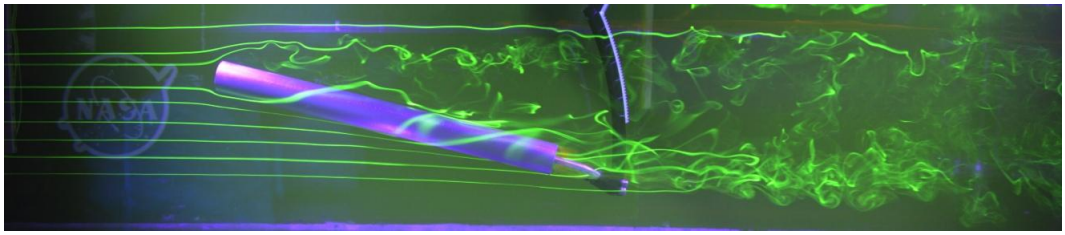

Figure 3D. Water channel results of the cylinder (side view).

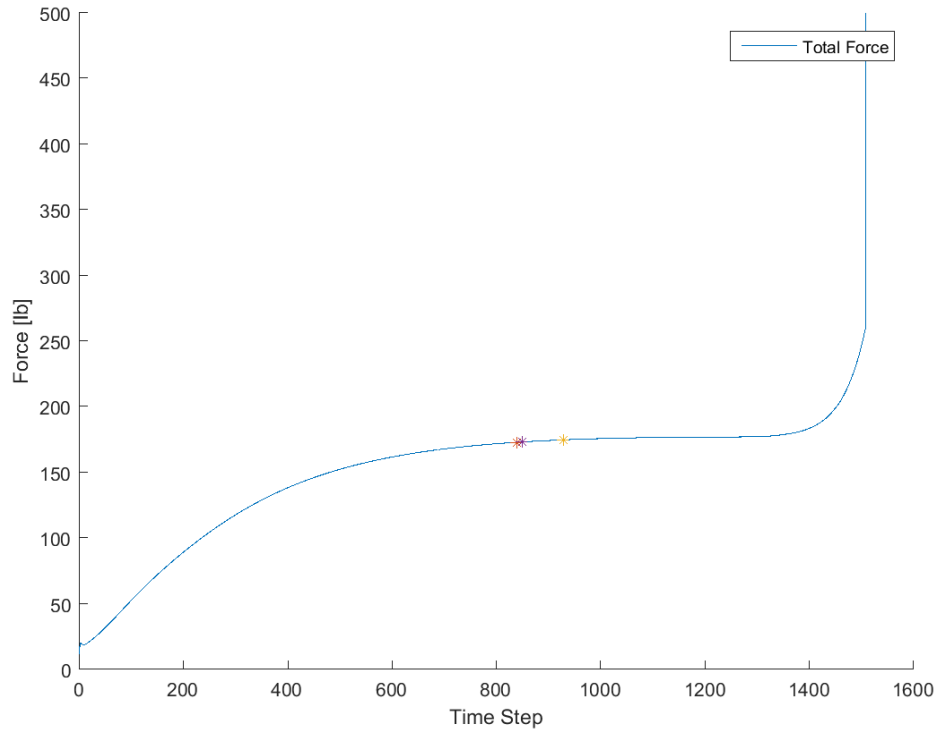

Figure 4. Total force against time steps for the turbulence relaxation study with turbulence relaxation factor 0.3.

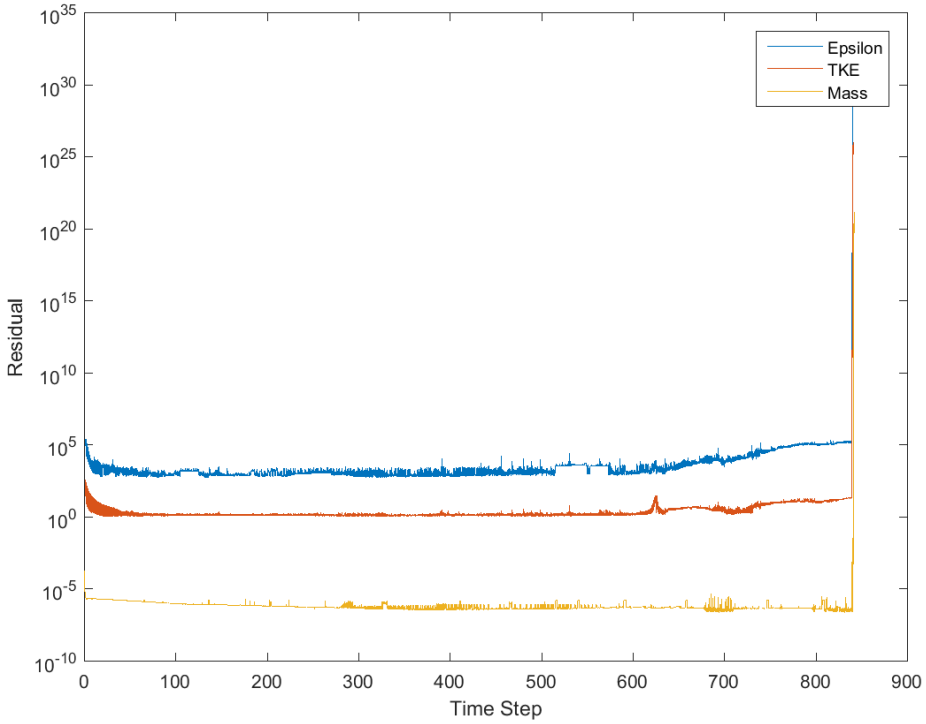

Figure 5. Residual plot for the initial turbulence relaxation factor 0.9/0.7.

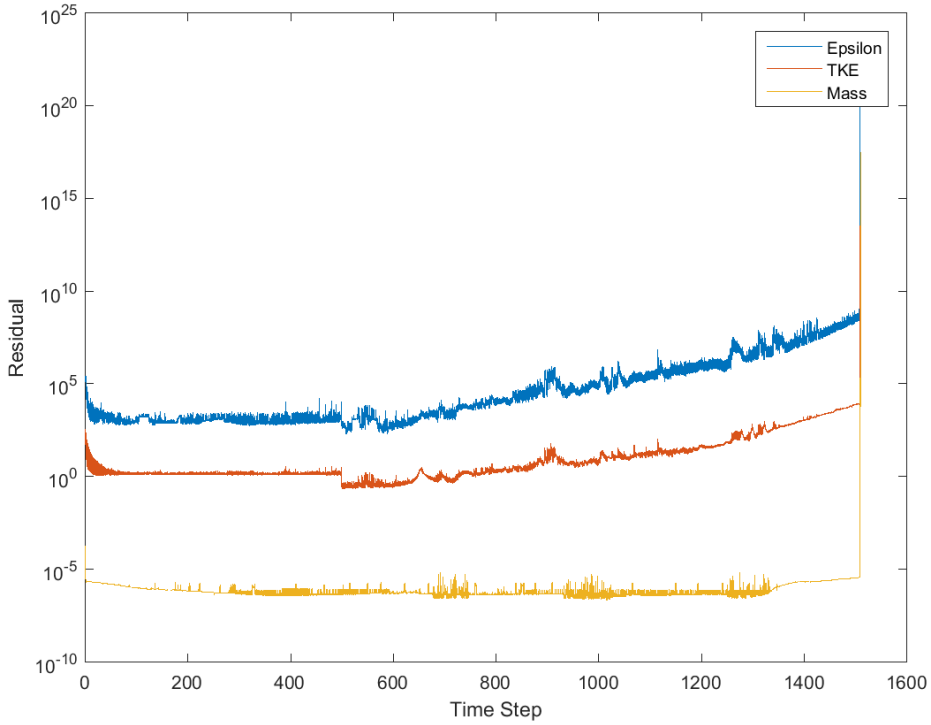

Figure 6. Residual plot for the turbulence relaxation factor 0.3.

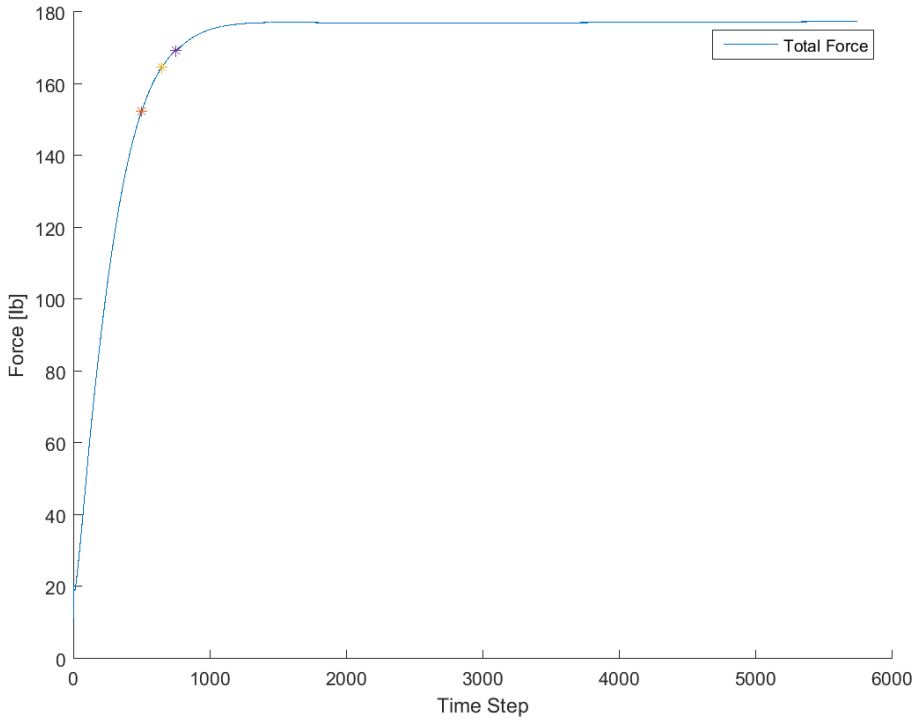

Figure 7. Total force against time steps for the time step size study with time step size decrements.

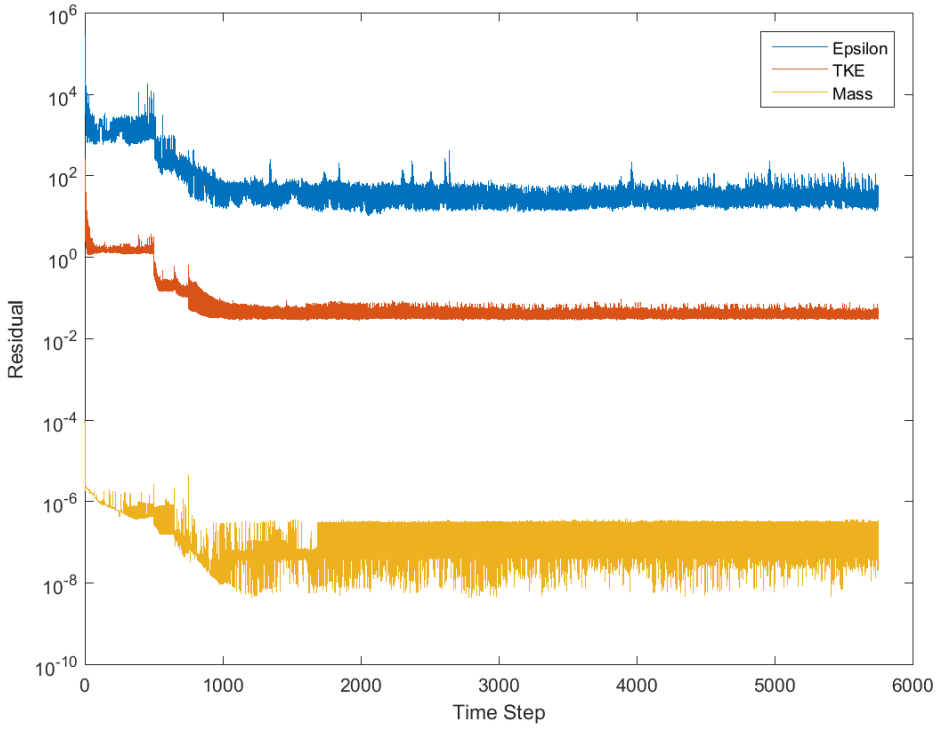

Figure 8. Residual plot for the time step size study with time step size decrements.

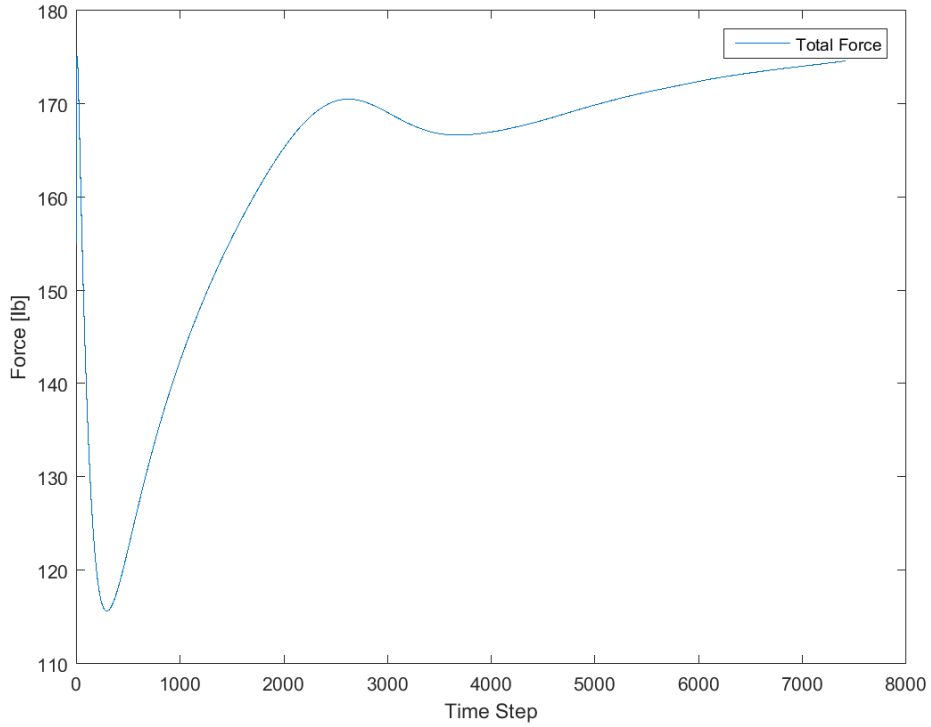

Figure 9. Total force against time steps for the time step size study without time step size decrements.

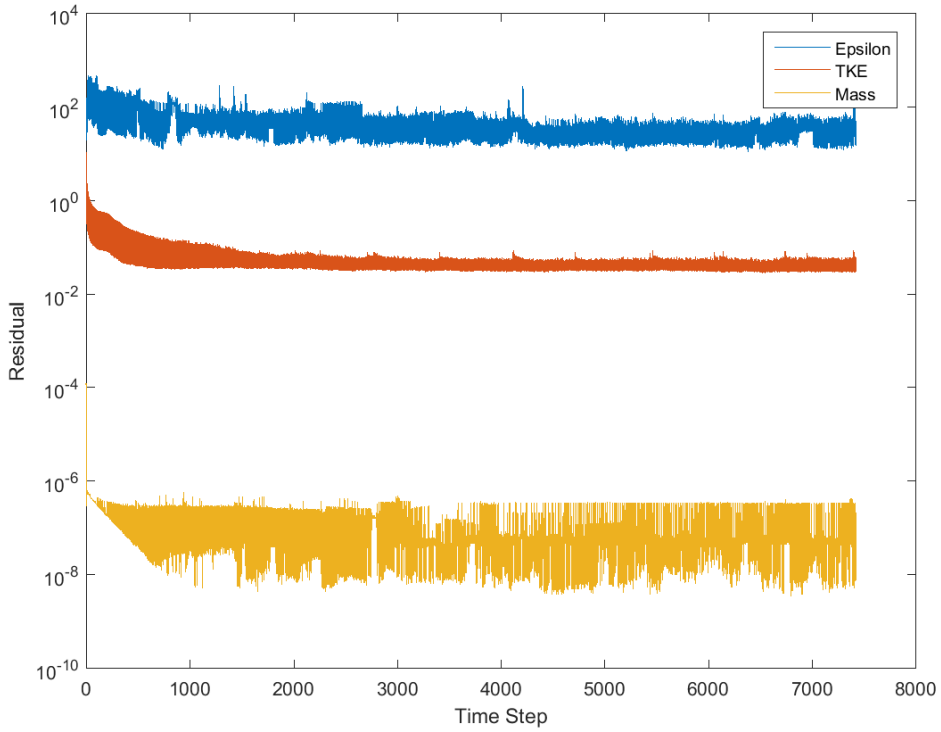

Figure 10. Residual plot for the time step size study without time step size decrements.

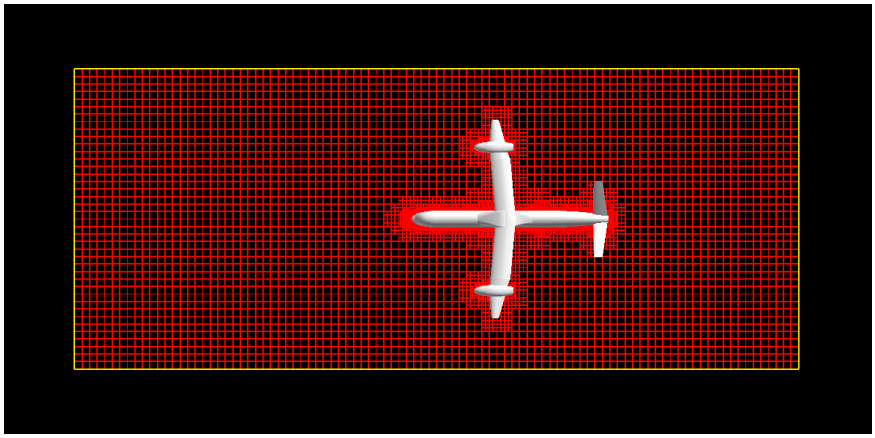

Figure 11. Grid of the LCTR in airplane mode at fuselage level in the 7- by 10-Foot Wind Tunnel.

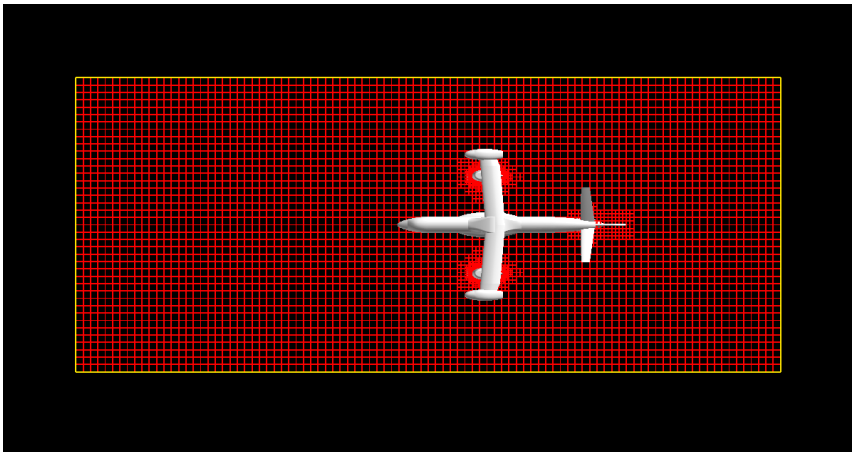

Figure 12. Grid of the LCTR in airplane mode without wing extensions at fairing level in the 7- by 10-Foot Wind Tunnel.

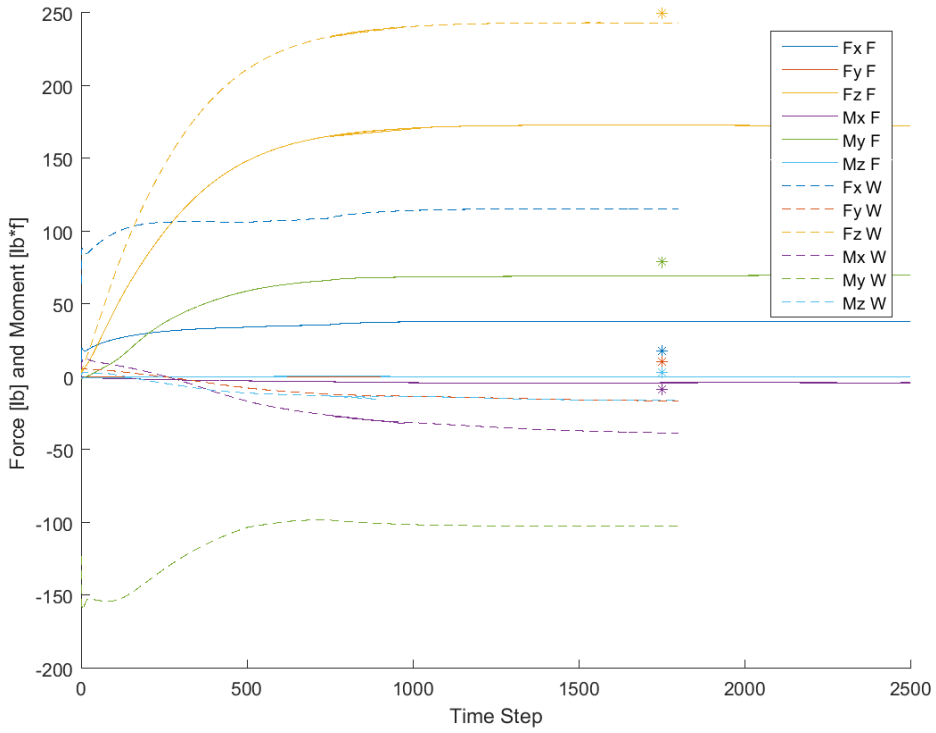

Figure 13. Forces and moments plot for the LCTR in airplane mode in freestream (F) and with wind tunnel walls (W).

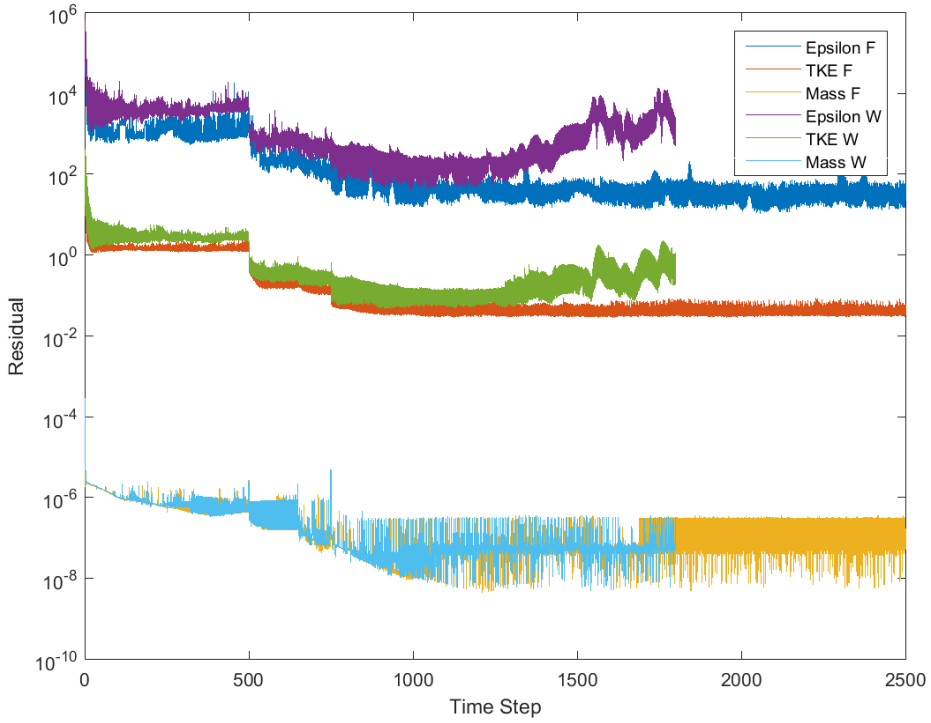

Figure 14. Residual plot for the LCTR in freestream and with wind tunnel walls.

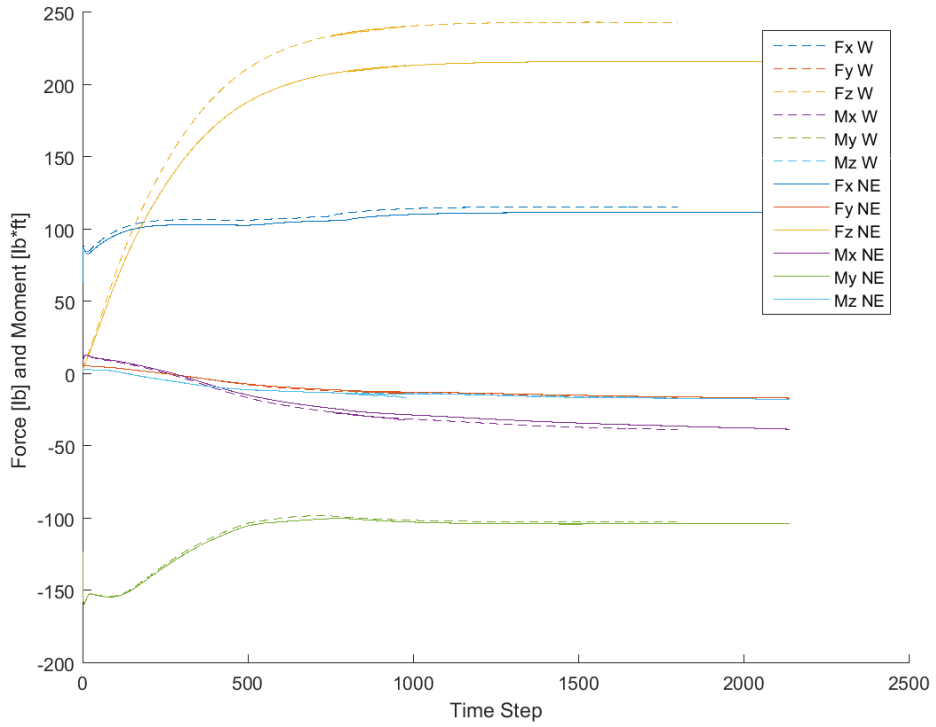

Figure 15. Forces and moments plot for the LCTR in airplane mode with wind tunnel walls, with (W) and without wing extensions (NE).

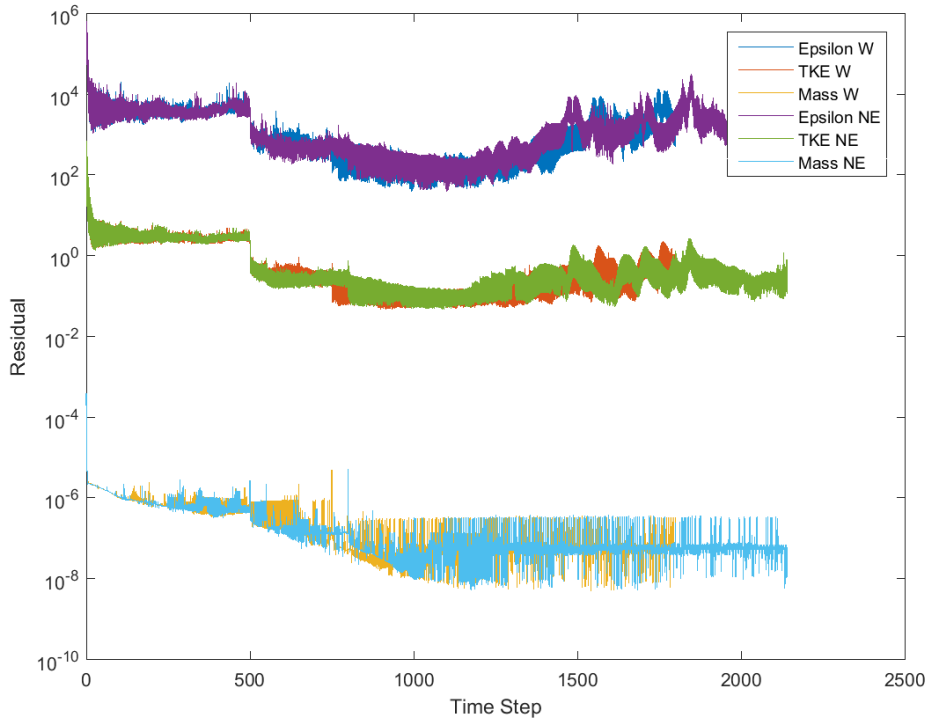

Figure 16. Residual plot for the LCTR with wind tunnel walls, with and without wing extensions.